Journal of Flow Control, Measurement & Visualization, 2022, 10, 99-116
https://www.scirp.org/journal/jfcmv
ISSN Online: 2329-3330
ISSN Print: 2329-3322

Quantitative Visualization of the Thermal Boundary Layer of Forced Convection on a Heated or Cooled Flat Plate with a 30° Leading Edge Using a Mach-Zehnder Interferometer

Jun Liu[1], Atsuki Komiya[2]

[1]Tochigi R&D Center, Keihin Corporation, Tochigi, Japan
[2]Institute of Fluid Science, Tohoku University, Sendai, Japan
Email: liujun3@hotmail.com

How to cite this paper: Liu, J. and Komiya, A. (2022) Quantitative Visualization of the Thermal Boundary Layer of Forced Convection on a Heated or Cooled Flat Plate with a 30° Leading Edge Using a Mach-Zehnder Interferometer. *Journal of Flow Control, Measurement & Visualization*, **10**, 99-116.
https://doi.org/10.4236/jfcmv.2022.104007

Received: December 26, 2021
Accepted: July 20, 2022
Published: September 30, 2022

Abstract

This study focuses on the experimental measurements of the heat transfer coefficient over a flat plate with a 30° leading edge. Under forced convection by a hot/cold air and flow over a cooled/heated flat plate, the thermal boundary layer and its thickness are quantitatively visualized and measured using a Mach-Zehnder interferometer. In addition, the variation in the local heat transfer coefficient is evaluated experimentally with respect to the air flow velocity and temperature. Differences within the heat transfer performance between the plates are confirmed and discussed. As a result, the average heat transfer performance is about the same for the heated plate and the cooled plate under all air velocity conditions. This contrasts with the theoretical prediction in the case of low air velocity, the reason considered was that the buoyancy at the 30° leading edge blocked air from flowing across the surface of the plate.

Keywords

Thermal Boundary Layer, Forced Convection, Heat Transfer Coefficient, Visualization, Mach-Zehnder Interferometer

1. Introduction

Heat transfer by convection, natural convection, forced convection, and mixed convection are common processes. Forced convection is the most popular method within thermal engineering applications based on its high heat transfer rate. Thus, accurate determination of the heat transfer coefficient is important in

many industrial applications. For example, based on the rapid spread of electric vehicles, thermal management simulations have become increasingly more important due to the lack of a sufficient heat source [1]. In addition, more detailed heat transfer processes need to be considered in the development and design of subsystem, such as the heating, ventilation, and air conditioning systems in vehicles [2] [3]. To improve the simulation accuracy of temperature fields, it is necessary to determine an accurate heat transfer coefficient for the boundary conditions of thermal simulation models.

Thus, many analytical and numerical studies on thermal boundary layers in forced convection have been conducted on the well-known case of a flat plate. Watkins [4] presented numerical solutions for the unsteady thermal boundary layers—in an incompressible laminar flow—over a semi-infinite flat plate for several Prandtl numbers. Shu and Pop [5] studied a steady forced convection thermal boundary layer over a flat plate with a predefined surface heat flux both analytically and numerically. Vigdorovich [6] investigated a turbulent thermal boundary layer on a permeable flat plate with transpiration. Kandula *et al.* [7] performed three-dimensional simulations on a thermal boundary layer over a flat plate with surface temperature discontinuity. Aziz [8] presented a similar solution for a laminar thermal boundary layer over a flat plate under convective surface boundary conditions. Recently, a novel method for describing the thickness and shape of a thermal boundary layer utilizing probability density moments was developed by Weyburne [9].

Experimental research on convective heat transfer issues over flat plates has mainly been conducted on velocity boundary layers. However, there have been a few experimental studies on thermal boundary layers in forced convection over a flat plate. He *et al.* [10] measured the heat transfer rates in laminar and turbulent boundary layers using thin-film heat transfer transducers. Leontiev *et al.* [11] obtained experimental results for the heat transfer in air flows past models with different configurations of vortex reliefs in the form of spherical dimples on plane surfaces. Wu *et al.* [12] experimentally investigated the convective heat transfer characteristics of a flat plate using a wind tunnel and electrical heating method. Shoji *et al.* [13] developed a phase-shifting interferometer to visualize the thermal boundary layer over a heated flat plate.

However, engineering applications are the most intriguing targets in terms of the differences in the heat transfer coefficient between the cooling of a heated plate and vice versa. The quantitative visualization of thermal boundary layers is important for accurately determining the heat transfer coefficient. In this study, for forced convection over a heated or cooled flat plates, the thermal boundary layer was quantitatively visualized, and the thickness profile was precisely measured using a 3-dimensional Mach-Zehnder interferometer [14], and the local heat transfer coefficient and local Nusselt number across the plate were experimentally evaluated with respect to variations in free air flow velocity and temperature. In addition, the heat transfer characteristics were compared between

the heated and cooled plates, and the heat transfer coefficient of mixed convection was estimated by combining natural convection and forced convection, especially under the conditions of low air velocity.

2. Thermal Boundary Layer over a Flat Plate

When air flows over a flat plate, a thermal boundary layer is formed when the temperature of the air flow is different from the temperature of the surface of the flat plate. The convective heat transfer rate from or to the surface is expressed by Newton's law of cooling or heating as

$$q_{conv} = h\left|T_{wall} - T_{air}\right| \tag{1}$$

where, q_{conv}, h, T_{wall} and T_{air} are the convective heat transfer rate, the heat transfer coefficient, the temperature of the surface of the plate and the temperature of air flow, respectively.

Because the velocity of the air flow is zero at the surface of the plate, the heat transfers between the surface of the plate and the air flow layer adjacent to the surface can be considered as pure conduction and the conductive heat transfer rate is given by

$$q_{cond} = k_{air}\left|\frac{\partial T}{\partial y}\right|_{y=0} \tag{2}$$

where, q_{cond} is the conductive heat transfer rate, k_{air} is the thermal conductivity of the air flow, and y is the vertical coordinate of the flat plate (see Figure 1 for the coordinates x and y).

Based on the principle of thermal energy conservation, the local heat transfer coefficient at point x over the plate h_x can be obtained as

$$\left(q_{conv}\right)_x = \left(q_{cond}\right)_x \xrightarrow{\text{yields}} h_x = \frac{\left(k_{air}\right)_x \left|\frac{\partial T}{\partial y}\right|_{x,y=0}}{\left|T_{wall} - T_{air}\right|_x} \tag{3}$$

where, x is the horizontal coordinate of the flat plate, and the subscript x means

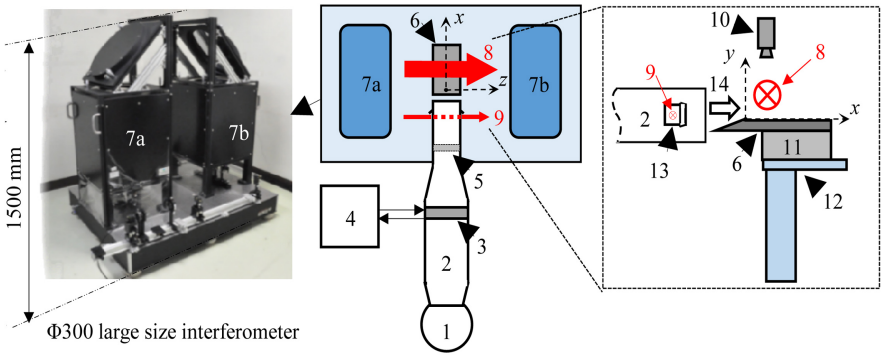

Figure 1. Layout of experimental apparatus. 1: blower, 2: duct, 3: heat exchanger, 4: water heater & cooler, 5: rectifier, 6: flat plate, 7a, 7b: Mach-Zehnder interferometer, 8: test beam, 9: reference beam, 10: thermographic camera, 11: Peltier unit, 12: support, 13: beam pass hole, 14: air flow.

the local value at point x. Therefore, to quantify the local heat transfer coefficient at point x over the plate under forced convection, it is necessary to determine the temperature gradient at point x on the surface of the plate.

In addition, to evaluate the difference in heat transfer characteristics between the heated and cooled plate, the average Nusselt number ($\overline{Nu}$) over the plate is introduced as

$$\overline{Nu} \equiv \frac{1}{L_m}\int_0^{L_m} Nu_x \mathrm{d}x = \frac{1}{L_m}\int_0^{L_m} \frac{h_x \cdot x}{(k_{air})_x}\mathrm{d}x \tag{4}$$

where L_m is the measured length along the flat plate, Nu_x is the local Nusselt number at point x over the plate.

3. Experimental Apparatus and Procedure

A Mach-Zehnder type interferometer was applied to visualize the thermal boundary layer along a flat plate. A flat plate with a 30˚ leading edge was fabricated from aluminum to avoid influence of the plate tip thickness on air flow. The thickness, width along the optical axis, and length along the wind direction were 5 mm, 60 mm, and 110 mm. A schematic of the experimental apparatus is shown in **Figure 1**. Conventionally, boundary layer thickness is often measured on the side opposite from the 30˚ leading edge cut. However, because it is difficult to keep the air flow inside a duct parallel to the plate in our experimental apparatus, we examine whether the boundary layer could be visualized on the edge cut side.

Figure 2 shows the schematics of 3-dimensional interferometer applied in this study. Basic arrangement of the interferometer is Mach-Zehnder type, yet the optical path is designed in 3 dimensional to enlarge an aperture (view area) at least 300 mm in diameter, in which a distribution of thermal boundary thickness on a flat plate can be clearly visualized. Conventionally, the interferometers used to apply two concave mirrors to scale up the visualization area size, however, the aberration problem limits the size while the size becomes larger by only the use of two mirrors compared with conventional interferometers. The proposed interferometer has adopted a lens system instead of mirror system [15]. **Figure 2(A)** shows a schematic of optical path in top view, and **Figure 2(B)** shows that in lateral view. A He-Ne laser (the wavelength = 632.8 nm) is used as the optical source. The laser is linearly polarized at an angle of π/4 with respect to the horizontal plane. The laser intensity was precisely controlled by a ND filter. The laser beam then passes through a spatial filter, consisting of an objective lens and a pinhole, to reduce the spatial noises of the optical source. The denoised beam passes through a convex lens and is collimated. The first beam splitter installed in the left-hand side in **Figure 2** splits the beam into test and reference beams. The test beam travels in the upward direction and after passing through a beam expander (*i.e.* lens system shown as (h) in **Figure 2**), becomes a 300 mm diameter beam. Alternatively, the reference beam travels straight through a half-wave plate, and after reflection in a mirror, goes upward. The beam diameter does not

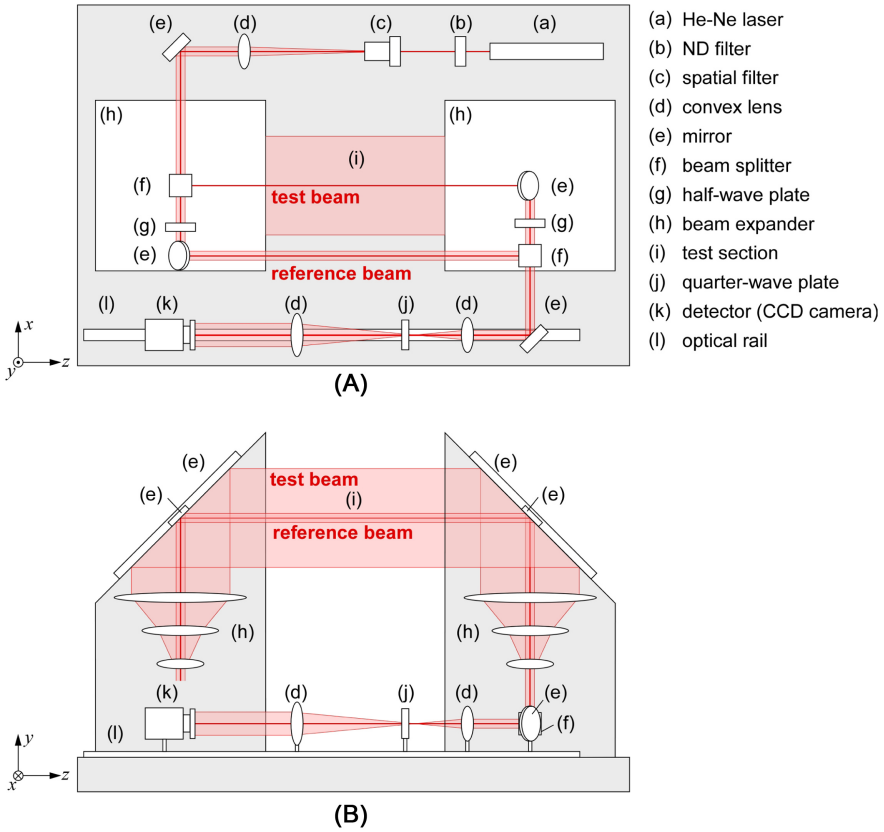

Figure 2. Schematics of 3-dimensional Mach-Zehnder type interferometer.

expand but keeps original diameter. The mirrors at the top of left-hand side tower are fixed at a 45˚ tilt, and both two beams travel horizontally. Only the test beam passes through a test section, and then they travel downward after reflection at 45˚ tilt mirrors fixed at the top of right-hand side tower. At the bottom of the tower, the shrunk test beam passing through a half-wave plate and reference beam are combined by another beam splitter. Since the polarized planes are perpendicular each other, two beams do not interfere. The combined beam then passes through a quarter-wave plate and a fringe pattern showing a density profile can be obtained.

From the visualized image, the refractive index distribution of the fluid in the vicinity of flat plate was firstly obtained. This fringe image shows the density distribution of the fluid. In this experiment series, no mass transfer occurs near the plate. Additionally, there is no pressure distribution in fluid region. As is obvious that the refractive index is a function of temperature, concentration and pressure, so this causes that the density distribution obtained from experiment is directly converted to that of temperature. Eventually, the temperature distribution could be obtained from the fringe image.

The experimental procedure can be summarized as follows.

1) A Peltier unit was utilized to heat or cool the lower surface of the flat plate with an attachment length of 10 mm along the air flow direction until a uniform temperature distribution on the upper surface was achieved. The surface of the

flat plate was coated with a thin black tape (thickness of 0.2 mm), excluding the contact area of the Peltier unit. This was done in order to stabilize the time variation of the plate temperature.

2) The temperature of the water circulator in the heat exchanger was controlled by the water heater and cooler so that the air flow through the heat exchanger can reach the target temperature, and the velocity and temperature of the air flow were measured at the outlet of the duct in advance.

3) After the start of air blowing, the air that was heated or cooled by the heat exchanger and flows toward the flat plate. Simultaneously, interference fringe photographs of the reference beam and test beam with UHD-4K resolution (3840 × 2160 pixels) were captured continuously for 2 s using a digital camera (SONY *α*7-II). The shutter speed of the camera was 1/3500 s and the data sampling rate was 5 fps. The temperature distribution on the upper surface of the plate was also continuously recorded by an infrared camera (Optris PI 450i), its accuracy is ±2% for temperature ranges −20˚C - 100˚C and exceptional thermal sensitivity is 40 mK.

Two sets of experimental conditions were considered (see Table 1).

The room temperature and relative humidity were maintained at 20˚C and 40%.

4. Results and Discussion

Prior to the discussion of the visualization experiment, the temperature uniformity of the flat plate is to be evaluated. This is because in the front region of plate, where the Peltier unit is not attached, is considered to be a fin. The uniformity is validated by calculating the plate's Biot number and fin efficiency from Equations (5) and (6). Value of the Biot number smaller than 0.1 means that the temperature profile in the plate is uniform, and the fin efficiency close to 1 indicates uniformity of the upper surface temperature.

$$Bi = \frac{hd_t}{k_w} = 1.31 \times 10^{-3} \tag{5}$$

$$\xi = \frac{1}{\sqrt{\frac{hpl^2}{k_w S}}} \frac{J_1\left(\sqrt{\frac{2hpl^2}{k_w S}}\right)}{J_0\sqrt{\frac{2hpl^2}{k_w S}}} = 0.99 \tag{6}$$

Table 1. Experimental conditions.

case	Peltier unit (˚C)	Water heater & cooler (˚C)	Target velocity of air flow (m/s)
cold air flow over a heated plate	75	0	2 - 12
hot air flow over a cooled plate	0	80	2 - 12

where the heat transfer coefficient h is assumed to be 49 W/m^2/K [16], d_t (=5 mm) is the thickness of plate, l (=100 mm) is the fin length where the Peltier unit is not attached, p (=10 mm) is the fin perimeter of the leading edge, S (=300 mm^2) is the cross-sectional area, k_w (=203 W/m/K) is the thermal conductivity of the plate, and J_0 and J_1 are the zeroth-order and first-order Bessel functions of the first kind, respectively.

Furthermore, the surface temperature distributions of the plate are measured using an infrared camera with frame rate 50 Hz. Figure 3 presents the temperature distributions along the centerline (z = 0) of the flat plates, and Figure 4 plots the average temperature of the x direction (x = 0 - 40 mm) along z-axis for the two experimental conditions. One can see that the variation in surface temperature is 1 to 2 K. Therefore, the surface temperature is assumed to be uniform throughout our experiments, it also means that the air flow is uniform in the z direction over the flat plate.

4.1. Visualization of Thermal Boundary Layer

The visualization of a thermal boundary layer near the flat plate is successful in a

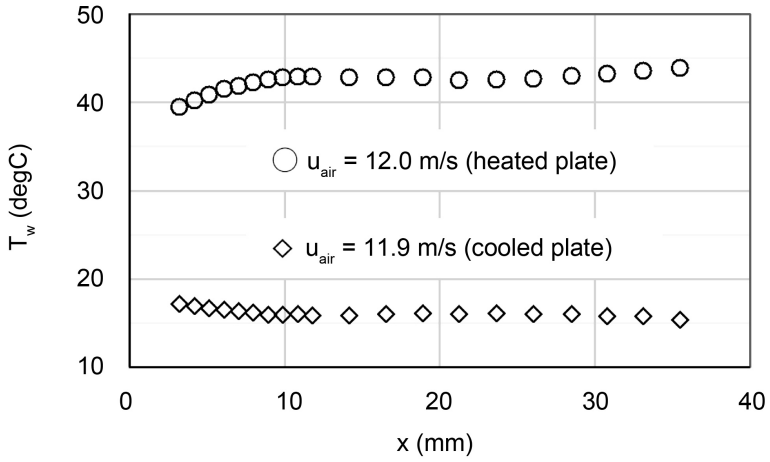

Figure 3. Surface temperatures along the centerlines of the flat plate.

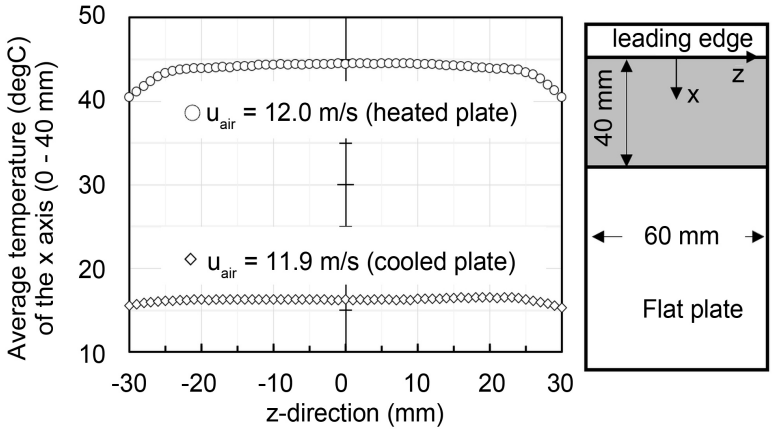

Figure 4. Average temperatures of x axis changes along z-direction.

visualization area with a length of 55 mm along *x*-direction and a width of 20 mm along *y*-direction, and the resulting red-black (RB) images have a maximum brightness of 256 (values of 0 to 255). This value is related to the data process of a detector. In this study, we applied an 8-bit digital camera, so the maximum brightness was fixed to 256. For example, **Figures 5(A)-(D)** present several instantaneous visualizations of the temperature field with interference fringes appearing in the vicinity of the plate. Because the natural convection occurs on the heated plate even in the absence of air flow, the interference fringes are only visible around the heated plate as shown in **Figure 5(A)**. **Figure 5(C)** and **Figure 5(D)** display the temperature field on the thermal boundary layer with interference fringes appearing in the case of forced convection by airflow. However, the influence of natural convection on the thermal boundary layer should be considered. The effects of this natural convection will be discussed later. Only the fringes appearing on the upper surface of the plate are considered in this study.

In addition, it can be seen that the temperature profile becomes unstable and fluctuates instantaneously in the rear area of the flat plate as the air velocity increases, as shown in **Figure 6**, which presents several instantaneous visualizations of the temperature field under the same experimental conditions. The interference fringes are evidently different in the rear area of the plate, because the 30˚ leading edgecauses airflow separation and reattachment on the flat plate, thus the boundary layer transforms from laminar to turbulent [16]. A type of slowly recirculating aircalledalaminar separation bubble [17], formed between the points of separation and reattachment in the case of high air velocity, as shown in **Figure 7**.

4.2. Evaluation Method for Thermal Boundary Layer

Theoretically, a thermal boundary layer can also be defined (similar to the velocity boundary layer) as the distance from the surface to the point at which the temperature is within 90% to 99% of the temperature difference between fluid

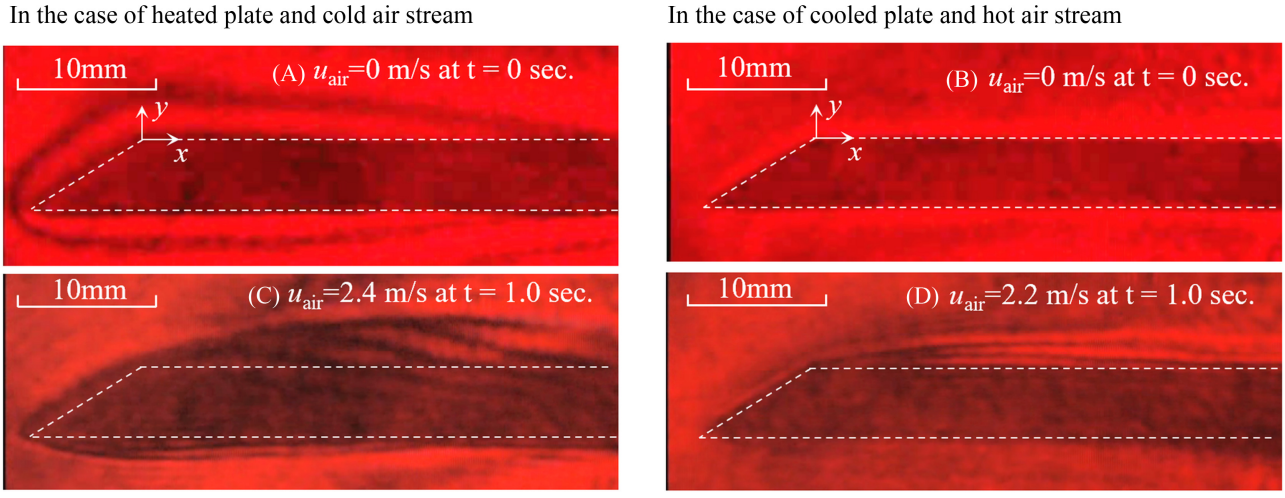

Figure 5. Instantaneous visualization of temperature field around the plates.

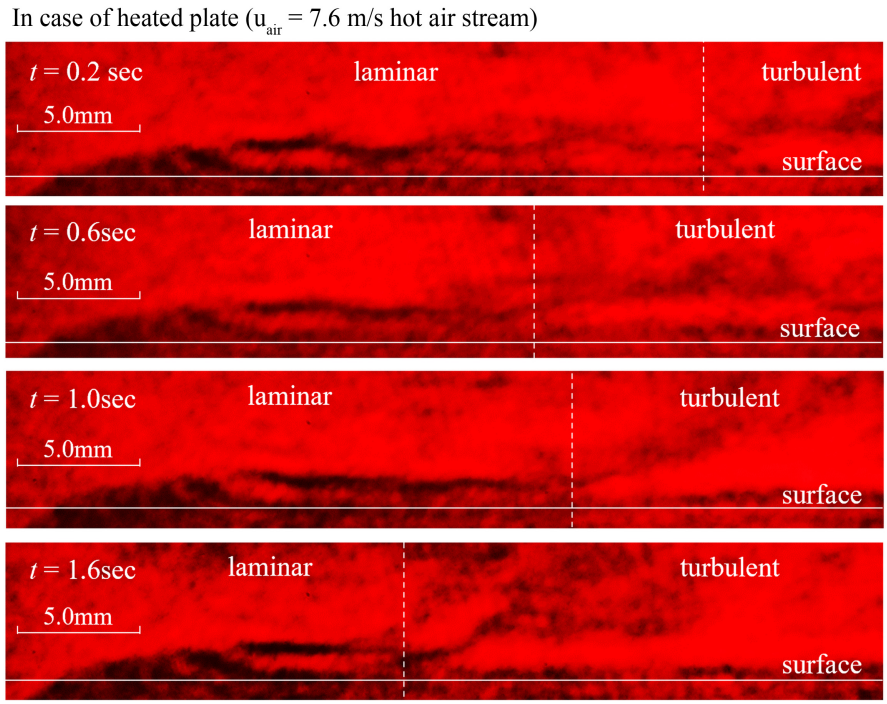

Figure 6. Instantaneous visualization of temperature field on the surface of plate.

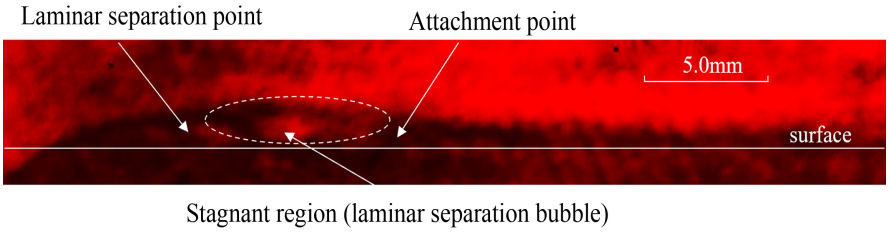

Figure 7. Airflow separation and reattachment in the case of a heated plate with cold air (u_{air} =12 m/s).

and wall. In the study, 90% of temperature difference was applied to determine the thickness of thermal boundary later. Therefore, it is necessary to precisely determine the temperature distribution in the vicinity of hot/cold wall in our experiments. In the case of a cooled plate with a hot air flow velocity of 2.7 m/s, four interference fringes are identified near the plate as shown in **Figure 8(A)**, outside of which there is a heat sink at a uniform ambient temperature. **Figure 8(B)** plots the image brightness data from 10 columns along the normal direction of the plate in the evaluation region, and the red circle is the average value of the brightness data in columns. The position of the outermost interference fringe which is defined as the final change from a black to a red image is indicated by the dashed line. Because the interference fringes correspond to isotherms, the temperature profile within the thermal boundary layer can be obtained from the number of fringes and two boundary conditions, such as the surface temperature of the plate and ambient temperature (see the paper by Torres *et al.* [14] for details). Therefore, the temperature at the outermost fringe,

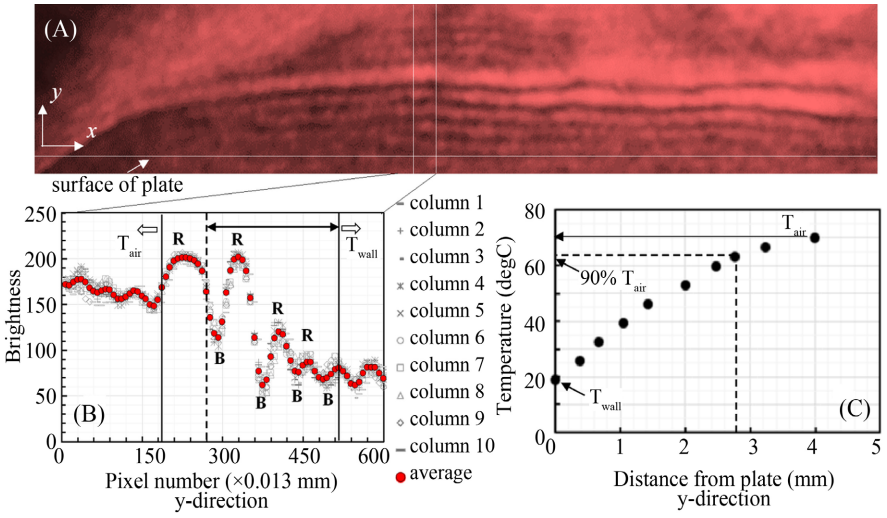

Figure 8. Temperature profile of the thermal boundary layer.

which can be clearly determined, is approximately 90% of the ambient temperature, as shown in Figure 8(C). In our experiments, one wavelength (dark → bright → dark → bright) has a brightness value of 256, so the theoretical temperature resolution under the experimental condition is 0.048 K by Equation (7) without experimental error. And the spatial resolution is 0.013 mm, which is obtained by determining the pixel size of the corresponding image based on a reference scale.

$$\Delta T = \frac{\left|T_{wall} - T_{air}\right|}{\text{number of fringes} \times 256} \tag{7}$$

Figure 9 presents the method used to measure the thickness of the thermal boundary layer over plate based on the interference fringe. Past the end point of the leading edge, 20 evaluation sections perpendicular to the flat plate are considered, as shown in Figure 9(A), and the brightness variations of the interference fringe image along each section are evaluated. For example, Figure 9(B) presents the variations in brightness values along three sections. As the brightness value increases, the image changes from black to red. Conversely, the image moves from red to black as the brightness value decreases. The thermal boundary layer thickness is defined as the distance from the surface to the final change from a black to a red image. The thickness of the thermal boundary layer along the plate is presented in Figure 9(C).

4.3. Thickness of Thermal Boundary Layer and Local Heat Coefficient

Since the airflow separation and reattachment occur on the flat plate in the case of high air velocity, the local temperature gradient on the surface of the plate, which is defined in Equation (3), is divided into two cases: laminar and turbulent. On one hand, a stable temperature distribution profile can be obtained in the case of laminar flow and the theoretical temperature gradient [18], which is

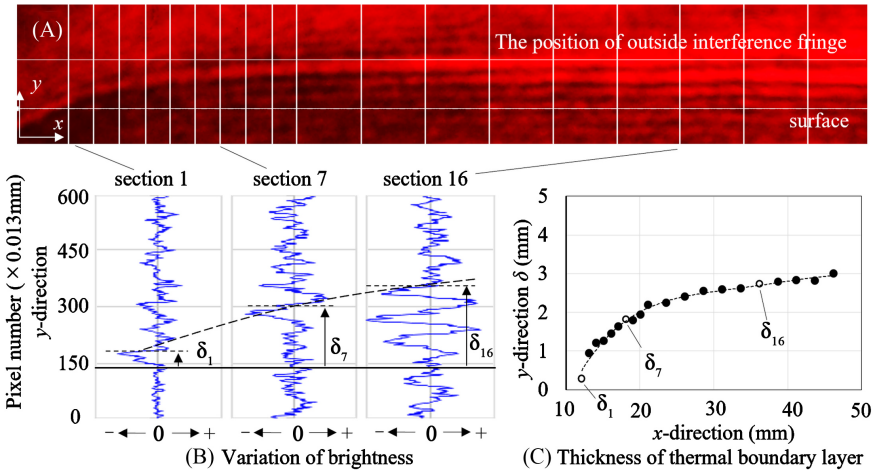

Figure 9. Definition of the thickness of the thermal boundary based on the interference fringe in case of cooled plate (hot air velocity u_{air} = 2.7 m/s).

as follows

$$\left|\frac{T-T_{wall}}{T_{air}-T_{wall}}\right|_x = \frac{3}{2}\left(\frac{y}{\delta_T}\right)_x - \frac{1}{2}\left(\frac{y}{\delta_T}\right)_x^3 \rightarrow \left|\frac{\partial T}{\partial y}\right|_{x,y=0} = \frac{3}{2}\left(\frac{\left|T_{air}-T_{wall}\right|}{\delta_T}\right)_x \tag{8}$$

where δ_T is the thickness of the thermal boundary layer. On the other hand, the temperature distribution profile is unstable in the case of turbulent flow, so the local temperature gradient on the surface of the plate is approximately calculated based on the distance (δ_1) between the first interference fringe and the plate, it is given as follows

$$\left|\frac{\partial T}{\partial y}\right|_{x,y=0} \approx \left|\frac{T_{wall}-T_{air\_\delta 1}}{\delta_1}\right|_{x,y=\delta_1/2} \tag{9}$$

where, δ_1 is the distance between the first interference fringe and the surface plate, and $T_{air\_\delta 1}$ is the air temperature at the first interference fringe.

To evaluate the influence of natural convection in the case of the heated plate, Richardson number (Ri) is utilized to represent the importance of natural convection relative to forced convection and is calculated as follows

$$Ri = \frac{Gr}{Re^2} = \frac{g\beta\left(T_{wall}-T_{air}\right)L}{u_{air}^2} \approx \begin{cases} 0.043 & \text{at } u_{air} = 2.5 \text{ m/s} \\ 0.005 & \text{at } u_{air} = 7.6 \text{ m/s} \\ 0.002 & \text{at } u_{air} = 12.0 \text{ m/s} \end{cases} \tag{10}$$

where, Gr and Re are Gash of number and Reynolds number, which represent the magnitude of buoyancy force and flow shear force, g is the gravitational acceleration, β is the thermal expansion coefficient of air, and L is the length of the flat plate. Typically, natural convection is negligible when $Ri < 0.1$, forced convection $Ri > 10$, and neither are $0.1 < Ri < 10$ [19]. However, in this study, it is found that the influence of natural convection can be neglected except in the case of u_{air} = 2.5 m/s. To evaluate the heat transfer coefficient over the heated plate, the h_x for natural convection [18] is given by

$$\left(h_x\right)_{natural} = \left(\frac{2k_{air}}{\delta_T Pr^{0.33}}\right)_x \tag{11}$$

where, Pr is Prandtl number. The h_x for forced convection is obtained by combining Equation (3) and (8), so the h_x for mixed convection over the heated plate can be considered by correlations as follows

$$\left(h_x\right)_{mixed} = \sqrt{\left(h_x\right)_{natural}^2 + \left(h_x\right)_{forced}^2} \tag{12}$$

Figure 10 presents the variation of the thickness of the thermal boundary layer across the flat plate under several conditions of air flow velocity. The local heat transfer coefficient across the flat plate is quantitatively evaluated as shown in Figure 11, and Figure 12 plots the variations of $\left(h_x\right)_{natural}$ and $\left(h_x\right)_{forced}$ over the heated plate in the case of $u_{air} = 2.5\ \mathrm{m/s}$, where the black circles represent the temporal average values of measured data, except for the two interference fringe photographs captured at times of 0.2 and 2.0 s. These photographs are unsuitable for obtaining similar interference fringes under the experimental conditions with low air velocity and high air velocity, respectively. The short lines represent 95% confidence interval error bars. One can see that the thermal boundary layer becomes thinner with increasing air velocity and its local thickness increases along the plate. Additionally, the magnitude of the local heat transfer coefficient increases with increasing air velocity, the local heat transfer coefficient then decreases to a constant value along the surface of flat plate in the case of low air velocity. In the case of high air velocity, the local heat transfer coefficient drops from the front edge of flat plate and exhibits a sudden jump in the middle of the plate, but then continues to decrease. This is because the

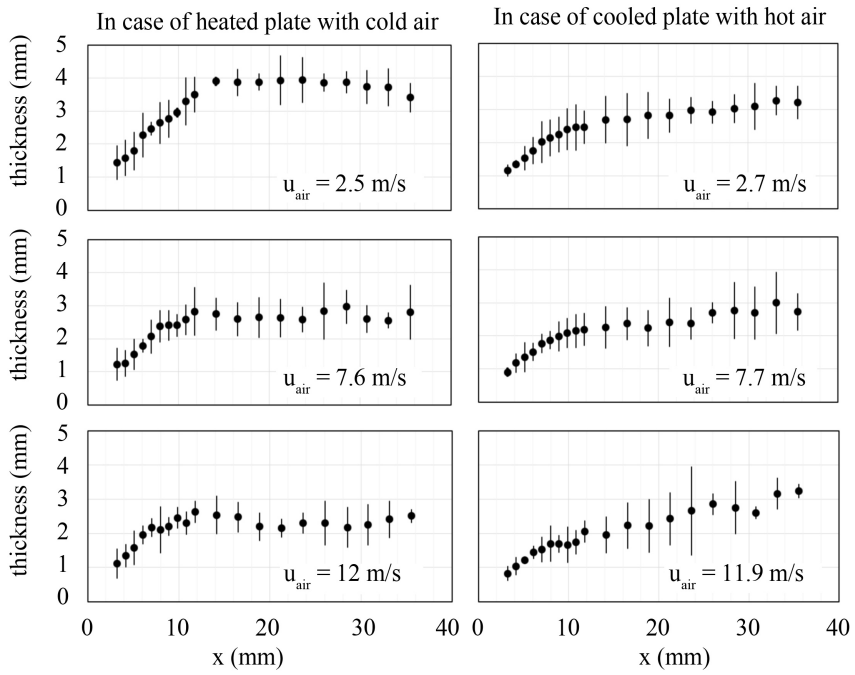

Figure 10. Thickness of the thermal boundary layer along the flat plate.

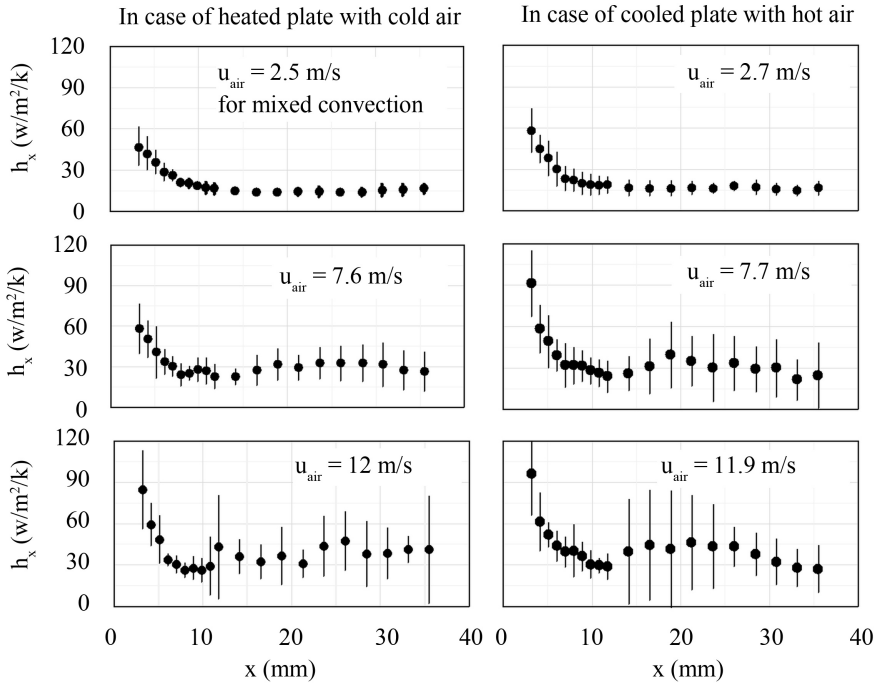

Figure 11. The local heat transfer coefficient along the flat plate.

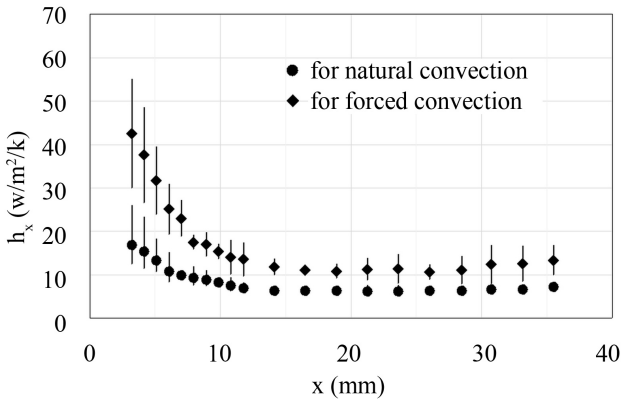

Figure 12. The variations of $(h_x)_{natural}$ and $(h_x)_{forced}$ over the heated plate in the case of $u_{air} = 2.5$ m/s .

turbulence after the reattachment of the airflow separation on the plate promotes heat transfer and yields a greater heat transfer coefficient, this change point moves closer to the leading edge of the plate as the air velocity increases. This variation trend in the experimental local heat transfer coefficient along the flat plate agrees with theoretical estimates [18].

4.4. Comparison of Heat Transfer Characteristics between Heated and Cooled Plates

Figure 13 presents the variation in the local Nusselt number along the surface of the flat plate, it indicates that the variation of experimental results follows almost the same trend as the theoretical prediction, which increases along the surface of

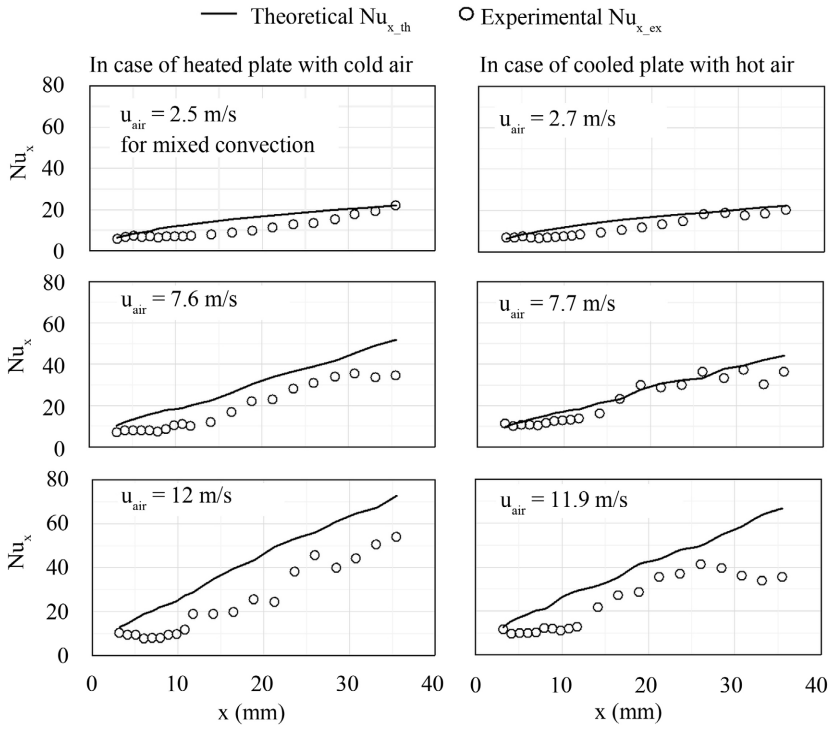

Figure 13. Local Nusselt number along the flat plate

the flat plate. However, in the case of high air velocity, an unchanging region appears in the front area of the flat plate, indicating that a constant heat transfer ratio may occur inside the laminar separation bubble as a result of airflow separation and reattachment on the plate.

The experimental Nu_{x_ex} and the theoretical Nu_{x_th} [18] are calculated as follows

$$Nu_{x\_ex} = \frac{x \cdot \left|\frac{\partial T}{\partial y}\right|_{x,y=0}}{\left|T_{wall} - T_{air}\right|_x} \tag{13}$$

$$Nu_{x\_th} = 0.332 \cdot Re_x^{0.5} \cdot Pr_x^{0.33} \quad \text{for laminar} \tag{14}$$

$$Nu_{x\_th} = 0.0296 \cdot Re_x^{0.8} \cdot Pr_x^{0.6} \quad \text{for turbulent} \tag{15}$$

where, Re_x and Pr_x are the local Reynolds number and local Prandtl number, which are evaluated based on the local air velocity and local temperature along the flat plate. The local air velocity divides into two cases of laminar and turbulent, which are defined by the cubic velocity profile for laminar flow and 1/7 power law of velocity for turbulent flowas

$$u_x = u_{air}\left[\frac{3}{2}\left(\frac{y}{\delta_u}\right) - \frac{1}{2}\left(\frac{y}{\delta_u}\right)^3\right]_x \quad \text{for laminar} \tag{16}$$

$$u_x = u_{air}\left(\frac{y}{\delta_u}\right)_x^{\frac{1}{7}} \quad \text{for turbulent} \tag{17}$$

where, δ_u is the thickness of the velocity boundary layer and the relationship with the thermal boundary layer δ_T is defined by Schlichting [20] as

$$\delta_u = \delta_T \cdot Pr^{0.33} \quad \text{for laminar} \tag{18}$$

$$\delta_u \approx \delta_T \quad \text{for turbulent} \tag{19}$$

As the case of $u_{air} = 2.5\ \text{m/s}$, similar to Equation (12), the Nu_{x_th} for mixed convection over the heated plate is given by

$$\left[Nu_{x\_th}\right]_{mixed} = \sqrt{\left(Nu_{x\_th}\right)^2_{natural} + \left(Nu_{x\_th}\right)^2_{forced}} \tag{20}$$

where, the theoretical Nu_{x_th} for forced convection equals Equations (14), and the theoretical Nu_{x_th} for natural convection [18] is as follow

$$\left(Nu_{x\_th}\right)_{natural} = 0.508 \cdot Gr_x^{0.25} \cdot Pr_x^{0.5} \cdot \left(0.952 + Pr\right)^{-0.25} \tag{21}$$

Figure 14 shows the average Nusselt number ($\overline{Nu}$) with air velocity increases from Equation (4), and the vertical lines represent 95% confidence interval error bars. One can see that the heat transfer capacities of heated plate and cooled plate are almost the same level in the case of larger air velocity because natural convection can be omitted. However, conventionally, the $\overline{Nu}$ value over the heated plate in the case of lower air velocity, which is the mixed convection, should be greater than that of a cooled plate with only forced convection. We believe that the difference from the theoretical prediction can be attributed to the buoyant force at the leading edge, which prevents air from flowing across the surface of the flat plate. Accordingly, that also can be found from Figure 10 and Figure 11, the thickness of thermal boundary layer and local heat transfer coefficient at the front of heated plate are thinker and smaller than that of cooled plate in case of lower air velocity.

5. Conclusion

In this study, the thermal boundary layer and its thickness under forced convection over a heated/cooled flat plate were quantitatively visualized and measured using a Mach-Zehnder interferometer. The variation in the heat transfer coefficient was experimentally evaluated with respect to the air flow velocity and

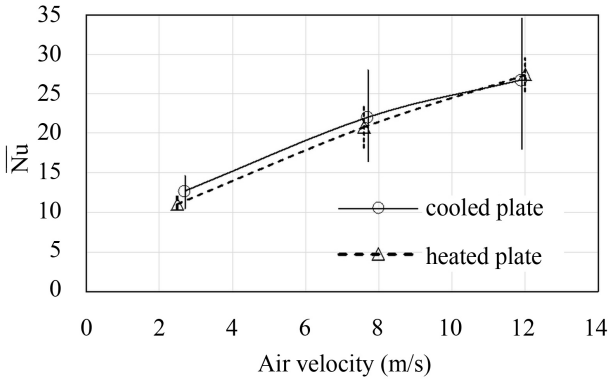

Figure 14. Comparison of average Nusselt number.

temperature. The experimental visualization of the thermal boundary layer on the flat plate was successful and the local heat transfer coefficient and local Nusselt number along the plate surface were quantitatively estimated. The experimental results for the flat plate were in good agreement with the theoretical predictions. When airflow separation and reattachment occurred in the front area of the plate in the case of high air velocity, the boundary layer thus transformed from laminar to turbulent over the plate and the local heat transfer coefficient then suddenly increased at the point of air reattachment. It was also observed that the local Nusselt number was small and almost unchanged in the region of the laminar separation bubble between airflow separation and reattachment. Additionally, the average heat transfer performances over the heated and cooled plates were, roughly to say, the same under all air velocity conditions, but it did not match the theoretical prediction for the case of low air velocity, due to the buoyant force at the leading edge prevented air from flowing across the surface of heated plate. In particular, regarding the mixed convection over the heated plate in the case of low air velocity, the local mixed heat transfer performance was calculated by combining natural convection and forced convection.

Conflicts of Interest

The authors declare no conflicts of interest regarding the publication of this paper.

References

[1] Yokoyama, A., Osaka, T. and Imanishi, Y. (2011) Thermal Management System for Electric Vehicles. *SAE International Journal of Materials and Manufacturing*, **4**, 1277-1285. https://doi.org/10.4271/2011-01-1336

[2] Umezu, K. and Noyama, H. (2010) Air Conditioning System for Electric Vehicles i-MiEV. *SAE Automotive Refrigeration System Efficiency Symposium* 2010, Scottsdale, 13-15 July 2010, 1-20.

[3] Bellocchi, S. (2018) Reversible Heat Pump HVAC System with Regenerative Heat Ex Changer for Electric Vehicles: Analysis of Its Impact on Driving Range. *Applied Thermal Engineering*, **129**, 290-305. https://doi.org/10.1016/j.applthermaleng.2017.10.020

[4] Watkins, C.B. (1975) Heat Transfer in the Laminar Boundary Layer over an Impulsively Started Flat Plate. *Journal of Heat Transfer*, **97**, 482-484. https://doi.org/10.1115/1.3450409

[5] Shu, J.J. and Pop, I. (1998) On Thermal Boundary Layers on a Flat Plate Subjected to a Variable Heat Flux. *International Journal of Heat and Fluid Flow*, **19**, 79-84. https://doi.org/10.1016/S0142-727X(97)10026-1

[6] Vigdorovich, I.I. (2007) Turbulent Thermal Boundary Layer on a Permeable Flat Plate. *Journal of Experimental and Theoretical Physics*, **104**, 972-988. https://doi.org/10.1134/S1063776107060155

[7] Kandula, M., Haddad, G.F. and Chen, R.-H. (2007) Three-Dimensional Thermal Boundary Layer Corrections for Circular Heat Flux Gauges Mounted in a Flat Plate with a Surface Temperature Discontinuity. *International Journal of Heat and Mass Transfer*, **50**, 713-722. https://doi.org/10.1016/j.ijheatmasstransfer.2006.07.008

[8] Aziz, A. (2009) A Similarity Solution for Laminar Thermal Boundary Layer over a Flat Plate with a Convective Surface Boundary Condition. *Communications in Nonlinear Science and Numerical Simulation*, **14**, 1064-1068. https://doi.org/10.1016/j.cnsns.2008.05.003

[9] Weyburne, D. (2018) New Thickness and Shape Parameters for Describing the Thermal Boundary Layer. arXiv: 1704.01120 [physics.flu-dyn].

[10] He, Y. and Morgan, R.G. (1994) Transition of Compressible High Enthalpy Boundary Layer Flow over a Flat Plate. *The Aeronautical Journal*, **98**, 25-34. https://doi.org/10.1017/S0001924000050181

[11] Leontiev, A.I., Kiselev, N.A., Burtsev, A.A., Strongin, M.M. and Vinogradov, Y.A. (2016) Experimental Investigation of Heat Transfer and Drag on Surfaces with Spherical Dimples. *Experimental Thermal and Fluid Science*, **79**, 74-84. https://doi.org/10.1016/j.expthermflusci.2016.06.024

[12] Wu, S.Y., Zhang, H., Xiao, L. and Qiu, Y. (2017) Experimental Investigation on Convection Heat Transfer Characteristics of Flat Plate under Environmental Wind Condition. *International Journal of Green Energy*, **14**, 317-329. https://doi.org/10.1080/15435075.2016.1259164

[13] Shoji, E., Nakaoku, R., Komiya, A., Okajima, J. and Maruyama, S. (2015) Quantitative Visualization of Boundary Layers by Developing Quasi-Common-Path Phase-Shifting Interferometer. *Experimental Thermal and Fluid Science*, **60**, 231-240. https://doi.org/10.1016/j.expthermflusci.2014.08.016

[14] Torres, J.F., Komiya, A., Shoji, E., Okajima, J. and Maruyama, S. (2012) Development of Phase-Shifting Interferometry for Measurement of Isothermal Diffusion Coefficients in Binary Solutions. *Optics and Lasers in Engineering*, **50**, 1287-1296. https://doi.org/10.1016/j.optlaseng.2012.03.006

[15] Shoji, E., Komiya, A., Okajima, J. and Maruyama, S. (2012) Development of Quasi Common Path Phase-Shifting Interferometer for Measurement of Natural Convection Fields. *International Journal of Heat and Mass Transfer*, **55**, 7460-7470. https://doi.org/10.1016/j.ijheatmasstransfer.2012.07.039

[16] Genc, M.S., Karasu, I., Acikel, H.H. and Akpolat, M.T. (2012) Low Reynolds Number Flows and Transition. In: Genç, M.S., Ed., *Low Reynolds Number Aerodynamics and Transition*, IntechOpen, Rijeka, 1-28. https://doi.org/10.5772/2398

[17] Mayle, R.E. (1991) The Role of Laminar-Turbulent Transition in Gas Turbine Engines. *Journal of Turbomachinery*, **113**, 509-537. https://doi.org/10.1115/1.2929110

[18] Incropera, F.P., Dewitt, D.P., Bergman, T.L. and Lavine, A.S. (2012) Principles of Heat and Mass Transfer. 7th Edition, John Wiley & Sons, Inc., Hoboken.

[19] Cui, P.Y., Li, Z. and Tao, W.Q. (2016) Wind-Tuel Measurements for Thermal Effects on the Air Flow and Pollutant Dispersion through Different Scale Urban Areas. *Building and Environment*, **97**, 137-151. https://doi.org/10.1016/j.buildenv.2015.12.010

[20] Schlichting, H. (1968) Boundary Layer Theory. 6th Edition, McGraw Hill, New York, 307.

Nomenclature

Bi = Biot number
d_t = thickness of plate
ΔT = temperature resolution
g = gravitational acceleration
Gr = Grash of number
h = heat transfer coefficient
h_x = local heat transfer coefficient over flat plate
J_0 and J_1 = zeroth-order and first-order Bessel functions of the first kind
k_{air} = thermal conductivity of air
k_w = thermal conductivity of plate
l = fin length of the leading edge
L = length of flat plate
L_m = measured length along the flat plate
Nu_{x_ex} = experimental local Nusselt number over flat plate
Nu_{x_th} = theoretical local Nusselt number over flat plate
$\overline{Nu}$ = average Nusselt number over flat plate
p = fin perimeter
Pr = Prandtl number,
q_{cond} = conductive heat transfer over plate
q_{conv} = convective heat transfer over plate
Re = Reynolds number
$\overline{Re}$ = average Reynolds number over flat plate
Ri = Richardson number
S = cross-sectional area
T_{air} = ambient temperature
$T_{air\_\delta 1}$ = air temperature at the first interference fringe.
T_{wall} = temperature at surface of plate
u_{air} = air flow velocity
x, y, z = Cartesian coordinate
β = thermal expansion coefficient of air
δ_1 = distance between the first interference fringe and the surface plate
δ_u = thickness of the velocity boundary layer
δ_T = thickness of thermal boundary layer
v = kinematic viscosity of air
ξ = fin efficiency of the leading edge